CORTEX 198 (2026) 137–154

Available online at www.sciencedirect.com

ScienceDirect

Journal homepage: www.elsevier.com/locate/cortex

Methods and Assumptions

Origin of neural frequency responses: Sensory coding versus structural influences

Ilker Duymaz [a,b,*], *Naoki Kogo* [c] *and Nihan Alp* [b]

[a] *Department of Mathematics and Computer Science, Physics, Geography, Justus Liebig University Giessen, Giessen, Germany*

[b] *Department of Psychology, Sabanci University, Istanbul, Turkey*

[c] *Department of Neurobiology, Faculty of Science, Donders Institute for Brain, Cognition and Behaviour, Radboud University, Nijmegen, the Netherlands*

ARTICLE INFO

Article history:
Received 7 October 2025
Revised 30 January 2026
Accepted 4 March 2026
Published online 11 March 2026

Keywords:
SSVEP
Visually evoked potentials
Frequency tagging

ABSTRACT

Periodic changes in visual input elicit rhythmic patterns in EEG signals that manifest as narrowband frequency components. These components are typically interpreted as signatures of neural populations sensitive to the modulated stimulus feature. We propose an alternative scenario in which such frequency components arise primarily from retinotopic variations in signal strength, without requiring feature-selective neural mechanisms. Using both simulated and empirical data (Experiment 1: $N = 13$; Experiment 2: $N = 13$), we demonstrate that signal fluctuations driven solely by the retinotopic position of a position-modulated stimulus can generate identifiable frequency components. These components are more plausibly attributed to structural properties of cortical organization that shape the relative contribution of different retinotopic areas to the EEG signal. Our findings challenge the conventional assumption that stimulus-related frequency components necessarily reflect feature-specific neural computations, indicating instead that functional interpretations are not guaranteed when spatiotemporal regularities in the stimulus introduce systematic population-level variability.

1. Introduction

Rhythmic changes in visual stimuli can induce corresponding rhythmic patterns in brain activity, which appear in EEG recordings as narrowband frequency components. When a visual or semantic stimulus property (e.g., contrast, object identity) is modulated at a specific frequency, neurons sensitive to that property tend to oscillate at the same or related frequencies, resulting in periodic fluctuations in EEG amplitude. By presenting the stimulus for a sufficient duration (e.g., longer than 1 sec; Norcia et al., 2015) and applying frequency-domain analyses, these periodic fluctuations can be identified as precise, narrowband frequency components. This phenomenon, known as the steady-state visually evoked potential (SSVEP; Regan, 1977), allows researchers to extract stimulus-related brain activity with a high signal-to-noise ratio (SNR). As a result, SSVEPs

* *Corresponding author*. Mathematics Institute, Justus-Liebig-University Giessen, Arndtstrasse 2, 35392 Giessen, Germany. (I. Duymaz)
E-mail address: ilker.duymaz@uni-giessen.de (I. Duymaz).

https://doi.org/10.1016/j.cortex.2026.03.005

have become a powerful tool for probing visual processing at multiple levels (Allen et al., 1996; Alp et al., 2016, 2018; Alp & Ozkan, 2022; Gundlach & Müller, 2013; Rossion et al., 2015), characterizing visual and neurological impairments (Sartucci et al., 2010; Silberstein et al., 2000), and developing brain-computer interface technologies (see Liu et al., 2022 for a review).

The distinctive inferential power of SSVEPs is rooted in the presumption that the precise frequency components evident in the data can be attributed to modulations in neuronal activity, typically interpreted as reflecting the brain's sensitivity to the periodically modulated stimulus feature, effectively tracking the activity of specific functionally specialized neural populations (Norcia et al., 2015). In theory, any other factor capable of inducing fluctuations in EEG amplitude could also give rise to such frequency components. However, for these fluctuations to be practically relevant, they must withstand the standard practices in experimental design and data processing that are typically used to filter out extraneous signals.

Of particular significance of these practices are extended trial durations and the averaging of data across multiple trials, which serve to accentuate visually evoked potentials by removing transient fluctuations that are not time-locked across trials (Trimble, 1968). Consequently, induced fluctuations must exhibit consistency within trials over time and synchronized phase across multiple trials to produce identifiable frequency components. Furthermore, given that SSVEP studies often focus exclusively on frequency components related to the modulation frequency of a periodically modulated stimulus property (Norcia et al., 2015), these fluctuations must also display periodic components that correspond to the stimulus modulation frequency and its harmonics.

Admittedly, it is challenging to envision any other factors capable of generating highly consistent signal fluctuations that are also sensitive to modulations in visual stimuli. This challenge has contributed to a prevailing interpretive stance that, since it is very unlikely to observe such narrow frequency components that are perfectly aligned with the periodicities of stimulus modulations, stimulus-related frequency components must reflect periodic engagement or modulation of functionally specialized neural populations (e.g., frequency-tagged face or object responses; Quek & Peelen, 2020; Retter & Rossion, 2016). Given the extensive array of low (e.g., contrast, motion direction) and high-level (e.g., face identity, object category) stimulus properties that can produce frequency components when modulated, this interpretive framework has become a conventional basis for linking narrowband responses to computations performed on the modulated feature, and alternative sources for these frequency components have received little consideration, as no compelling account has emerged in which any other factor could reliably introduce signal fluctuations that remain aligned with specific stimulus modulations.

Nonetheless, the magnitude of neuronal activity is not the only factor that determines the strength of measured EEG signals. Various other factors, such as the cortical volume (Schaul, 1998) and depth of the activated regions (Butler et al., 2019), dipole orientation of local currents relative to the electrode array (Capilla et al., 2016), the signal cancellation between simultaneously active brain areas (Ahlfors et al., 2010), and the thickness of the cerebrospinal fluid layer covering regions of interest (Rice et al., 2013), can impact the translation of cell activity into EEG signals. Under certain circumstances, such structural factors, as opposed to functional, can potentially interact with stimuli to introduce superficial influences into the data by modulating EEG amplitudes across conditions and/or time.

Particularly, position-dependent factors that introduce variances in the properties of different retinotopic populations can have a potentially large impact on recorded EEG signals by interacting with stimulus position. The visual field is not uniformly mapped onto the visual cortex (Allman & Kaas, 1971; Daniel & Whitteridge, 1961; Talbot & Marshall, 1941; Wandell et al., 2007). Significant differences exist in cortical volume and depth across retinotopic areas, depending on eccentricity and polar angle (Daniel & Whitteridge, 1961; Horton & Hoyt, 1991; Schwartz, 1980). When a stimulus is located in the periphery, a given portion of the visual field engages smaller and deeper neural populations (Daniel & Whitteridge, 1961; Horton & Hoyt, 1991; Schwartz, 1980). Similarly, population receptive field sizes are much smaller in foveal areas compared to peripheral ones, meaning that a central stimulus would engage a greater volume of neural tissue (Dumoulin & Wandell, 2008). As a result, the same stimulus can evoke larger or smaller EEG responses depending on the size and depth of the activated brain areas based on its position in the visual field (Slotnick et al., 2001).

For SSVEP studies in general, the modulation of EEG signals by such position-dependent factors does not directly warrant identifiable frequency components in the signal. In order to yield frequency components, these position-dependent factors would somehow have to induce consistent and phase-locked signal fluctuations across many repetitions of a condition. When stimuli are static, or when they do not follow a consistent pattern of motion across trials, it is highly unlikely for position-dependent factors to induce signal fluctuations that survive trial-averaging. However, if the position of a stimulus is periodically modulated in a consistent manner across trials, as is often the case in SSVEP studies involving moving stimuli (e.g., Aissani et al., 2011; Nozaradan et al., 2012; Pitchaimuthu et al., 2021; Varlet et al., 2023), these position-dependent imbalances may introduce consistent time-locked fluctuations in the signal, potentially giving rise to narrowband frequency components even after averaging signals across trials (Fig. 1).

In this context, we present a scenario in which stimulus-related frequency components emerge exclusively due to retinotopic variations in signal strength, rather than necessarily indicating periodic engagement or response modulation of functionally specialized, feature-selective neural populations. First, we use simulations to demonstrate that any sort of position-dependent variance in measured EEG responses can potentially introduce periodic signal fluctuations by interacting with position-modulated stimuli *even when the responses of local receptive units are driven equally*. If these fluctuations are discernible in actual EEG signals, they should manifest even in the absence of modulations in other stimulus properties, and must be strictly phase-coupled to modulations in stimulus position. In two subsequent EEG experiments, we demonstrate that periodically modulating the polar angle and eccentricity of a singleton stimulus induces frequency components when all

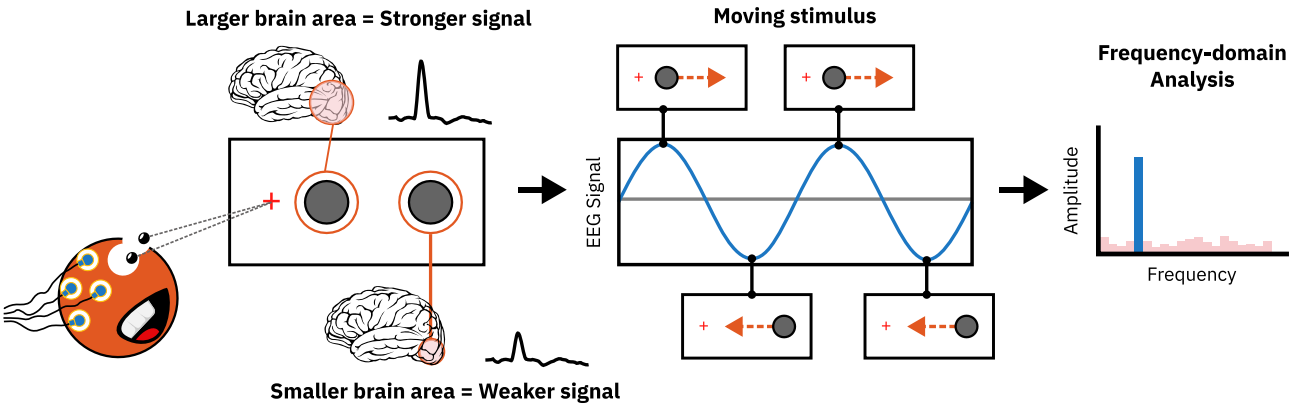

Fig. 1 – Frequency components arising from periodic position-dependent fluctuations. This figure illustrates a hypothetical situation based on eccentricity-related variations in cortical magnification (Daniel & Whitteridge, 1961; Horton & Hoyt, 1991; Schwartz, 1980). In the idealized scenario depicted by the gray line, we assume that equal-sized and equally dense cortical regions are allocated to different parts of the visual field and that, in addition, the effective gain from cortex to the EEG sensor (including electrode sensitivity and volume conduction) is uniform across positions. Under these assumptions, a singleton moving stimulus that drives a constant local neural response would generate a uniform, position-invariant signal at the sensor, resulting in a flat EEG time course (gray line). By contrast, if different regions of the visual field are represented disproportionately in the visual cortex, the same stimulus can lead to stronger or weaker measured signals depending on its position and the size of the corresponding cortical regions (blue line). When the stimulus position is periodically modulated, such position-dependent gain differences can introduce periodic fluctuations in the EEG signal, giving rise to identifiable frequency components even when individual neurons across positions are driven equally by the stimulus. For conceptual clarity, other realistic sources of position-dependent signal variation, such as spatial gradients in electrode sensitivity and non-uniform volume conduction, are not depicted here but would operate in an analogous manner.

other stimulus properties remain constant over time. Critically, these frequency components are eliminated through phase-cancelation when the phases of the position modulations are varied across trials.

If these frequency components were generated solely by functionally specialized neural mechanisms engaged by the stimulus (e.g., those sensitive to repeating movements), independent of its absolute position, they would have persisted even in the phase-varied conditions. Phase-cancelation in the phase-varied conditions suggests that these frequency components are phase-coupled to the position modulation of the stimulus, and therefore must strictly be related to fluctuations produced by position-dependent factors. Taken together, these results indicate that inherent retinotopic differences in measured EEG amplitude can autonomously introduce consistent, time-locked signal fluctuations in response to position-modulated stimuli, offering a counterexample to the conventional interpretive practice of attributing stimulus-locked frequency components primarily to functionally specialized neural mechanisms.

2. Simulation

It is conceivable to view the EEG signal as a comprehensive non-linear transformation on visual input. This transformation is the culmination of numerous layers of diverse non-linear processes introduced by the intricate machinery of neural processing, in addition to the physical factors that govern the translation of neuronal activity into EEG signals. For our purposes, we draw a clear distinction between two pivotal concepts: unit response and population-level response. Following this distinction, we will argue that while in a simplified unit-based framework, stimulus-related frequency components can arise from the responses of units that are sensitive to the modulated stimulus property, these components can also emerge at the level of population response independently of feature-sensitive unit activity. Our goal is not to claim that SSVEPs solely reflect the activity of narrowly feature-tuned neurons, but to contrast this standard feature-sensitivity description with an account in which structural factors at the population level are sufficient to generate stimulus-related frequency components. In our proposed population-level account, this emergence hinges on variances in the population response contingent upon the retinotopic stimulus position and the presence of a position-modulated stimulus.

We start by conceptualizing the unit response as an abstract representation of neuronal responses triggered by visual stimuli. In this context, the unit response characterizes a transformation of visual input, which we define as an arbitrary nonlinear function, denoted as $y = f(xs(t), \alpha(t))$. Here, y signifies the response amplitude of a unit responding to a stimulus whose position is xs and intensity α at time t. Our focus is not on modeling specific types of neurons, but rather on defining units that adjust their responses based on varying intensities of the stimulus properties to which they are tuned. Therefore, α (i.e., stimulus intensity) can be associated with

any stimulus property to which these hypothetical units are sensitive, and the function f can encompass various forms of neural computations.

Within this unit-based formalization, a common way to explain the frequency components observed in EEG signals in response to a periodically modulated stimulus is to assume that these frequency components arise from the nonlinear relationship between α and y. As long as f includes a non-zero coefficient for α, indicating sensitivity to changes in stimulus intensity, periodic modulation of α will invariably result in a periodic modulation of y. Consequently, if the stimulus intensity undergoes sinusoidal modulation, for example, it will induce a non-sinusoidal modulation of the unit response that repeats at the same time intervals as the stimulus modulation. As a result, the EEG signal will contain frequency components that are harmonics (integer multiples) of the sinusoidal stimulus modulation frequency, provided that an adequate number of units synchronously respond to the stimulus. This framework captures how feature sensitivity at the unit level can, in principle, generate stimulus-related frequency components. In the following, we show that analogous frequency components can also arise purely from retinotopic variations in population response strength, even when the underlying unit responses are driven equally by the stimulus.

Since our aim is to investigate whether identifiable frequency components can be generated independently of the unit response, specifically due to position-dependent variances in the responses of different retinotopic populations, we focus on the scenario in which the stimulus intensity α remains constant across time and the unit responses do not vary as a function of modulations in stimulus intensity. If a position-modulated stimulus, across its different positions, was processed by a perfectly homogenous ensemble of identical units without any position-dependent variability in the measured EEG strength, the resulting signal would not exhibit fluctuations and remain constant across time. This is because the stimulus would drive uniform responses from the same number of units with identical properties at each time point (Fig. 1, gray line). Conversely, if there are position-dependent factors that influence how unit responses translate into measured EEG strength, such as the density of units or their distance from the electrodes, the signal would exhibit fluctuations across different positions of the stimulus, even though individual local units receive the same information (i.e., stimulus intensity) and produce the same response. Moreover, if there are consistent variations in the receptive field properties of different retinotopic populations, these could also lead to position-dependent variability in EEG signals by modulating unit responses based on the pattern of overlap between the receptive fields and stimulus (Fig. 1, blue line).

To capture the effect of such position-dependent factors, we conceptualize population response as a representation of collective activity from many individual units responding to the stimulus as measured by the EEG. At each position of the stimulus, a number of units whose receptive fields overlap with the stimulus produce a response. The population response is a sum of responses from each of these units with weights determined as a function of the location of the unit's receptive field within the visual field:

$$Y(t) = \sum_{i=1}^{d(xs(t),\alpha(t))} g(x_i) \cdot f_i(xs(t), \alpha(t))$$

where d is a unit-density function that determines the number of units responding to a stimulus presented at retinotopic position xs with intensity α at time t; f is the magnitude of response for each unit responding to that stimulus; and g determines the extent to which the response of each unit contributes to the measured population response based on the location of its receptive field, x_i. Therefore, Y is the magnitude of the measured population response evoked by a stimulus whose position is xs and intensity α.

As our focus is solely on signal variations arising from position-specific factors, we assume that individual units produce identical responses when a stimulus with the same intensity α falls within their receptive fields. Therefore, we factor out the variance attributable to the correlation between individual unit responses and stimulus intensity under the condition that the intensity α is constant. However, unit responses would still vary depending on the extent of overlap between each unit's receptive field and the stimulus. Consequently, unit responses would exhibit variability contingent upon the positioning and dimensions of both their receptive fields and the stimulus. This inter-unit variance alone would not lead to differences in population response if the spatial distribution of units' receptive field sizes were identical for each population. Conversely, if the receptive field sizes of individual units, or their spatial distribution within the population receptive field, vary across populations, this could lead to differences in population responses along with other position-dependent factors. We account for this by keeping the $f_i(xs(t))$ term while excluding the variance attributable to α. Thus, we obtain:

$$Y(t) = \sum_{i=1}^{d(xs(t))} g(x_i) \cdot f_i(xs(t))$$

which denotes a stimulus-position-dependent coefficient for the magnitude of EEG signals recorded from a population of stimulated units, whose responses do not vary as a function of stimulus intensity but only as a function of the position of their receptive fields. It is then possible to calculate these position-dependent coefficients for stimuli encompassing arbitrary portions of the visual space (such as pixels on an image) at discrete time points and map them across the visual field. This produces a two-dimensional heatmap representing the variance in EEG amplitude caused by position-dependent factors, given otherwise uniform unit responses, which we refer to as Retinotopic Weight Function (RWF):

$$RWF_{u,v} = \sum_{i=1}^{d(xs_{u,v})} g(x_i) \cdot f_i(xs_{u,v})$$

The actual nature of the RWF is not of critical importance for our demonstration, and it can be substituted by any two-dimensional function that may or may not approximate the influence of biologically-plausible position-dependent factors on the EEG strength. The critical requirement for the RWF in

this context is that it consistently varies across the visual field and scales the contribution of each unit (to the signal) based on the location of their receptive fields. We will demonstrate that as long as this condition is fulfilled, position-dependent factors can interact with position-modulated stimuli to generate periodic signal fluctuations and therefore yield identifiable frequency components.

To this end, we simulate a hypothetical signal that contains only the fluctuations caused by position-dependent variances in population responses and not by the oscillations in unit responses induced by modulations in stimulus intensity. Therefore, we generate signals by multiplying a constant average unit response C with the respective position-dependent weight corresponding to the population response strength at each position of a moving stimulus.

$$S(t) = RWF_{x(t),y(t)} * C$$

where x and y are the cartesian coordinates of the stimulus position.

Given this framework, we explore three different cases for the RWF, as depicted in Fig. 2a–c. These RWFs were defined primarily for illustrative purposes, to span different types of spatial variation rather than to provide realistic models of the visual system. In Fig. 2a, the RWF decreases linearly with distance from the center; although this is an arbitrary choice, it loosely resembles eccentricity-dependent differences in cortical magnification that could, in principle, produce analogous variations in population response. In Fig. 2b, the RWF decreases linearly from left to right visual field and therefore introduces variation across polar angles, which can be seen as a simple example of anisotropic weighting. In Fig. 2c, the outputs of the RWF are randomly sampled from a uniform distribution on a fine spatial grid, thereby representing a complex spatially varying function without assuming any specific biological computation. Despite their arbitrariness, all three RWFs meet the essential condition of exhibiting consistent position-dependent differences in measured population responses, and thus serve to demonstrate that a wide range of non-uniform weighting functions can give rise to position-dependent frequency components.

Finally, we examine various forms of position modulation applied to a singleton stimulus (Fig. 2, Position Modulation column). First, we consider the rotational motion of a singleton object orbiting a central point (orbital). Second, we consider the repetitive translational motion of an object with a constant speed, which moves back and forth along a horizontal axis (linear). Third, we consider the position modulation of an object that blinks between two positions, akin to traditional long-range motion paradigms (blinking).

Fig. 2 (Signal column) illustrates the simulated signals generated for all combinations of three distinct RWFs and three types of position modulation (i.e., orbital, linear, and blinking). Signals were generated for 4-sec time windows with all three types of position modulation being repeated four times with a cycling frequency of 1 Hz. The simulated signals were then Fourier transformed to the frequency domain with a 1/4 = .25 Hz frequency resolution. All visible frequency components in the Frequency Domain column in Fig. 2 correspond to the harmonics of the position modulation frequency (i.e., 1 Hz).

In Fig. 2a, the RWF varies as a function of eccentricity. Consequently, the two position modulation types characterized by stable eccentricity over time (i.e., orbital and blinking), do not induce any fluctuations in the signal. In contrast, linear position modulation results in the stimulus traversing differently weighted retinotopic areas, thereby introducing fluctuations in the measured population response. These fluctuations repeat at the same temporal intervals as the periodic position modulation, giving rise to frequency components that are harmonics of the position modulation frequency. In Fig. 2b, the RWF decreases linearly from left to right. For orbital position modulation, this corresponds to a circular traversal of the stimulus through a linear range of weights, producing approximately sinusoidal fluctuations in the signal that exhibit primarily the fundamental position modulation frequency (1 Hz) in the frequency domain. By comparison, linear and blinking position modulations yield triangular and square-like waveforms, respectively, which characteristically exhibit odd harmonics of the fundamental frequency. In Fig. 2c, the RWF is substantially more complex. As a result, the generated signals appear more intricate than the simple waveforms in the previous two cases. Despite this complexity, the signals still produce frequency components that are harmonics of the position modulation frequency.

These simulations reveal that position-dependent disparities in measured population responses have the potential to interact intricately with position-modulated stimuli, giving rise to periodic fluctuations in the EEG signal. The characteristics of these fluctuations, including the frequency components they generate, are contingent upon both the RWF and the specific pattern of position modulation applied to the stimuli. Crucially, in our simulations, both the stimulus intensity and the magnitude of unit responses were considered identical for all local units responding to the stimulus across each timepoint. This means that the periodic fluctuations in our simulated signals do not stem from modulations in stimulus intensity and the consequent oscillations in unit responses that they induce, but rather are attributable to the position-dependent factors captured by the RWF.

These results pinpoint the hypothetical possibility of position-dependent factors inducing periodic fluctuations even when individual neurons across positions are driven equally by the stimulus. However, it is not clear whether these position-dependent factors have a practical influence on actual EEG signals. Therefore, to empirically investigate whether position-dependent factors could independently induce frequency components, we conducted two EEG experiments. Given that the fluctuations produced by position-dependent factors in our simulations are inherently phase-locked to the position modulation of the stimulus, we posited that these frequency components would persist after time-domain averaging when combining trials with identical phases for the position modulation. Conversely, we expected them to diminish when combining trials with varied phases

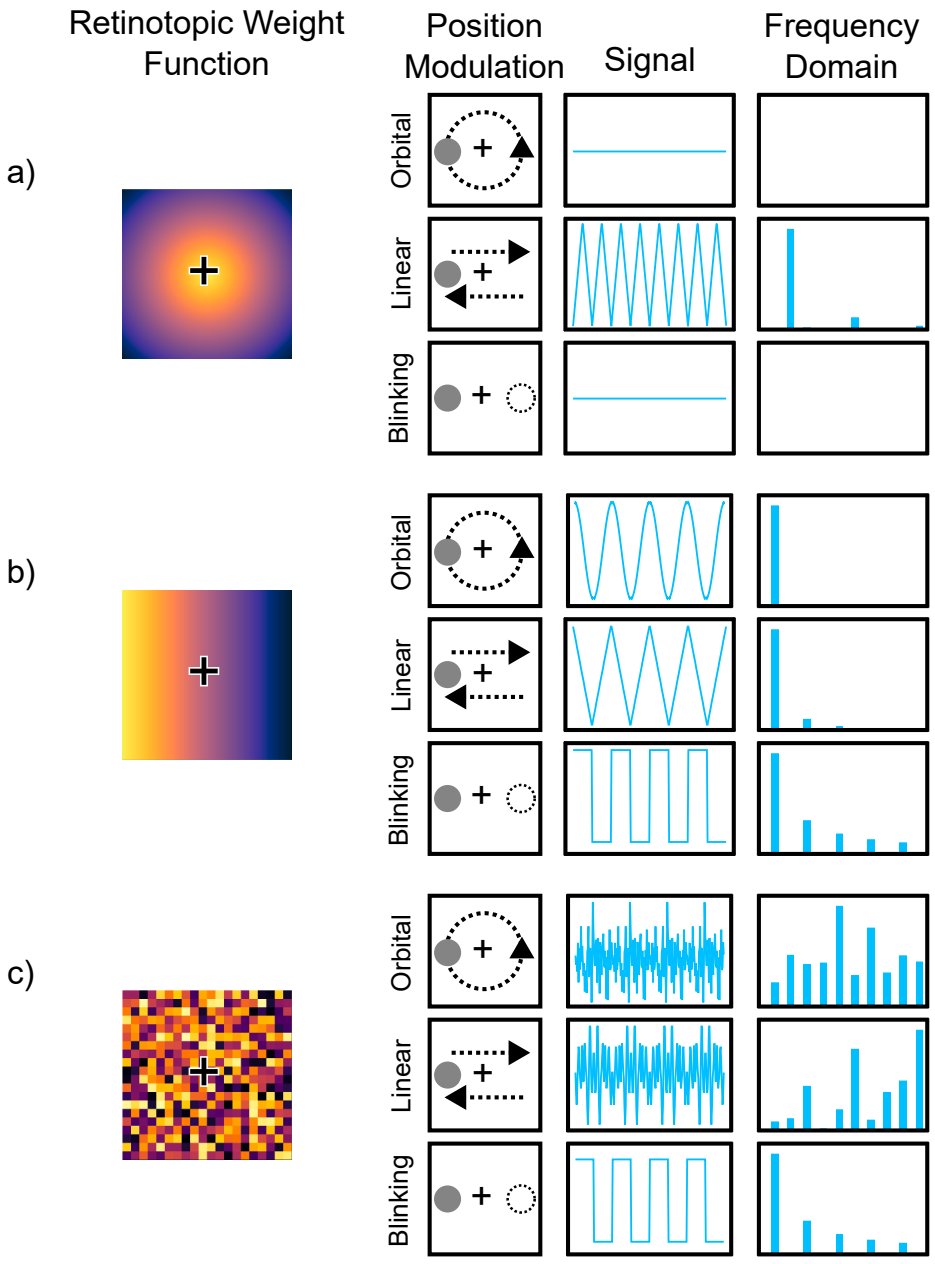

Fig. 2 – Simulated signals and their frequency domain representations. The Retinotopic Weight Function (first column) interacts with the type of position modulation (second column: Orbital, Linear, Blinking) to shape the time domain response (third column) and resulting frequency content (last column). Frequency domain responses (last column) show harmonics of the position modulation frequency. (a) Retinotopic Weight Function decreases linearly with eccentricity. Orbital position modulation: The singleton stimulus traverses along a circular path with constant eccentricity, which does not introduce fluctuations in the signal and does not lead to any frequency components. Linear: Stimulus eccentricity is linearly modulated along a horizontal line. The course of the eccentricity modulation is reversed sharply at the center and during motion-direction reversals (left-to-right, right-to-left). This is reflected in the signal as a triangular wave, which contains harmonics of double the position modulation frequency. Blinking: The singleton stimulus alternates between two locations that have identical weights in the Retinotopic Weight Function, therefore it also does not produce fluctuations and frequency components. (b) Retinotopic Weight Function decreases linearly from left to right visual field. Orbital: The signal is the projection of a circular motion along a linear gradient, which by definition is sinusoidal. Therefore, only the fundamental position modulation frequency is represented in the frequency domain. Linear: Stimulus seesaws along the axis of linear Retinotopic Weight Function gradient. The signal exhibits sharp reversals when the stimulus changes direction. This triangular signal contains the odd harmonics of the position modulation frequency. Blinking: Stimulus alternates between two locations with different weights, leading to a square wave signal and harmonics of the position modulation frequency. (c) Retinotopic Weight Function is randomly determined. Orbital and linear position modulation: The stimulus traverses through areas with randomly determined weights for the Retinotopic Weight Function. The consequent

for the position modulation. Therefore, we separately modulated the polar angle (Experiment 1) and eccentricity (Experiment 2) of a singleton dot, and incorporated both phase-locked and phase-varied conditions, in which the phases of these modulations were either stable or randomized across trials.

3. Experiment 1: Polar angle modulation

3.1. Materials and methods

In Experiment 1, we investigated whether the modulated polar angle of a singleton stimulus could interact with position-dependent factors to produce distinct frequency components when other stimulus properties are kept constant.

3.1.1. Participants

Fourteen Sabancı University students (8 female, 6 male; mean age = 21.1 years, SD = 2.02) with normal or corrected-to-normal vision participated in Experiment 1 for course credit. One participant's data was excluded from all analyses due to software errors during the recording session, reducing our sample size to 13. The sample size was based on previous studies with similar methods (e.g., Nozaradan et al., 2012; Pitchaimuthu et al., 2021; Varlet et al., 2023). A sensitivity analysis conducted using GPower software (Faul et al., 2007) revealed that this sample size was sufficiently powered (power = .80) to detect large effect sizes (Cohen's f > .42) for our within-subjects factors (see, 3.1.6 Frequency domain analysis). All procedures in this study were reviewed and approved by the Sabancı University Research Ethics Council. Participants gave informed consent prior to the experiment session.

3.1.2. Apparatus and stimuli

Stimuli were generated using PsychoPy (Peirce et al., 2019) and presented on an ASUS XG248Q monitor (23.8″, resolution = 1920 × 1080) with a refresh rate of 60 Hz. Participants viewed the stimuli from a 76.5 cm distance in a dark and quiet room. The stimuli consisted of a single light gray (contrast = 75%) dot rotating around a fixation cross on a dark gray (contrast = 25%) background. The dot had a radius of 1 dva and an eccentricity of 5 dva from the fixation cross. The dot always completed one full rotation in exactly 1 sec and had a constant movement speed with a 6°polar angle shift per motion frame. Trials lasted 11 sec, during which the dot completed 11 full rotations.

The rotational motion of the dot meant that its polar angle was modulated as a function of time. The phase of this polar angle modulation depended on the position from which the dot started its rotation. In one condition, the dot's rotation always started from the same predetermined polar angle chosen randomly for each participant from a range of 0°–350° in steps of 10° (e.g., 50° for one participant, 130° for another). The constant starting polar angle led to a phase-locked manipulation of the dot's polar angle across trials (Fig. 3a). We will hereafter refer to this condition as the phase-locked (PL) condition. In the second condition, the starting polar angle was randomly selected for each trial from the same range (0°–350° in steps of 10°) without replacement (i.e., each step was used only once). Since the dot started its rotation from a different polar angle on each trial, the polar angle modulation was not phase-locked in this condition (Fig. 3b). Therefore, we will refer to this condition as the phase-varied (PV) condition. There were 72 trials for each phase condition (PL and PV).

The only difference between the two phase conditions was the locked versus varied phase of the polar angle modulation. All other stimulus properties, including motion speed, direction-switch rate, rotational frequency, and eccentricity were identical between the two conditions. Moreover, these properties were either not expected to induce periodical signal fluctuations as they were not periodically modulated (e.g., motion speed) or were expected to yield identical frequency components in both conditions as their modulations were phase-locked in all trials (e.g., direction-switch rate, rotational frequency). For example, even when the dot started its rotation from different angles, it repeated its rotation cycle at exactly 1 sec intervals (i.e., rotational frequency). Likewise, the dot's movement direction was shifted by the same amount at each frame regardless of its starting polar angle (i.e., direction-switch rate). Therefore, we expected that any differences between the frequency components extracted from the two phase conditions would primarily stem from the phase manipulation applied to the polar angle modulation.

Since we were interested in EEG activity sensitive to polar angle modulation, we expected rotation direction to be a defining factor in the profile of the modulated EEG signal. Therefore, we also manipulated the rotation direction of the dot. In both phase conditions, the dot rotated either clockwise (CW) or counterclockwise (CCW), counterbalanced within each condition. Hence, we had 36 CW and 36 CCW trials for each phase condition.

3.1.3. Procedure

Each trial started with a fixation cross displayed on a gray background for 1 sec, followed by an 11-sec presentation of the rotating dot stimulus. After each trial, there was a self-paced break in which the participants pressed a keyboard key to proceed with the next trial. In approximately 14% of the trials (12 trials per block), the rotating dot briefly changed its color for 250 msec at a random time (except during the first and last seconds of the trial). Participants were instructed to fixate on a red cross at the center of the screen, and press keys on the keyboard whenever they noticed a change in the dot's color ("F" key if the dot turned red, "J" if it turned green). The trial was terminated upon

signals are highly complex, but since they have the same period as the position modulation cycle, they contain harmonics of the position modulation frequency in their frequency domain representations. Blinking: Stimulus alternates between two locations with different weights similarly to (b). The square wave signal contains the harmonics of the position modulation frequency.

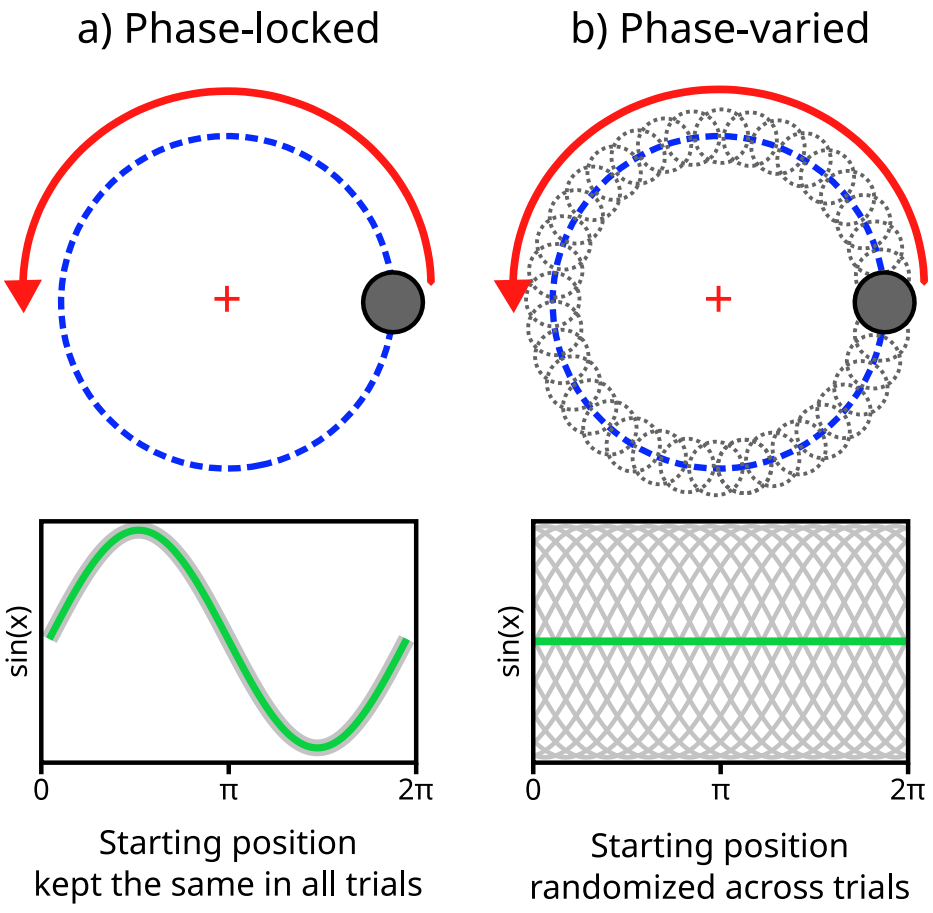

Fig. 3 – Phase manipulation of the polar angle modulation. (a) In the phase-locked condition, the dot consistently initiated its rotation from the same polar angle across trials, resulting in a consistent phase for the polar angle modulation. The sine functions (green lines) in the second row are provided for illustrative purposes, demonstrating how the dot's starting angle influences the phase of the polar angle modulation. Although the actual signal evoked by the polar angle modulation may not be sinusoidal, its phase is expected to align with the phase of this modulation. (b) In the phase-varied condition, the dot's starting angle was randomly chosen on each trial from the 36 predefined polar angles. Consequently, the polar angle modulation was not phase-locked across trials in the phase-varied condition, which would result in non-phase-locked signals canceling out each other when averaged in the time domain (the straight green line).

response or after the 1-sec response window, with a feedback (i.e., correct/incorrect) text displayed for 1 sec. These trials acted as catch trials to motivate participants to pay attention to the stimulus.

Trials from PL and PV conditions were presented in two separate blocks, the order of which was counterbalanced between participants. Each block consisted of 72 experimental and 12 catch trials, with an equal number of CW and CCW trials, in random order. Participants took a 3–5 min break between the two blocks. Prior to the experiment, participants completed a short practice block (2–3 min) of 12 catch trials to get accustomed to the task.

3.1.4. *EEG acquisition*

EEG was recorded using 64 Ag/AgCl active electrodes placed on the scalp according to the international 10-10 system (ActiCAP, Brain Products GmbH, Gilching, Germany) with the following modifications: The channels TP10 and FT10 were placed above and below the participants' right eye to be used as vertical electrooculogram (VEOG) channels, and TP9 was used to replace the otherwise absent Iz channel. BrainVision Recorder software (Brain Products GmbH, Gilching, Germany) was used to record the EEG data at a 1000 Hz sampling rate with channel impedances kept below 20 kΩ.

3.1.5. *EEG preprocessing*

Fieldtrip Toolbox (Oostenveld et al., 2010) and custom scripts were used to preprocess the data. A fourth-order Butterworth bandpass filter (.5–100 Hz) was applied to the continuous data. Power line noise was removed by a multi-notch filter at frequencies 50, 100, and 150 Hz with bandwidths of 1, 2, and 3 Hz, respectively. The online reference channel (FCz) was re-added to the data and channels were re-referenced to the average of all channels. Blink artifacts were removed by implementing an Independent Component Analysis (ICA) in Fieldtrip, using

EEGLAB's runica algorithm (Delorme & Makeig, 2004). Bad channels were determined by visual inspection and interpolated (.37% per participant on average) using neighboring channels. Data were then segmented into 11-sec trial epochs and downsampled by a quarter to 250 Hz for computational efficiency. A small number of trials were rejected ($M = 1.38\%$, $SD = 2.38$) due to hardware-related artifacts (peak amplitude >500 μV). Data from the catch trials were excluded from all analyses.

3.1.6. *Frequency domain analysis*

We expected position-dependent discrepancies in EEG strength to induce periodic fluctuations in the signal by enhancing or attenuating the strength of the population response at different polar angles of the rotating dot stimulus. Therefore, we expected the phases of these periodic fluctuations to align with the phase of our polar angle modulation. Consequently, we anticipated these fluctuations to exhibit phase-locking across the trials of our PL condition, but not across the trials of the PV condition.

To extract the periodic fluctuations induced by the polar angle modulation, we utilized time-domain averaging and averaged the trials from each of our conditions in the time domain (Trial $N \approx 36$). Time-domain averaging eliminates noise while keeping phase-locked signals intact (Trimble, 1968). As a consequence, we expected time-domain averaging to preserve the polar angle modulation frequencies in the PL condition, but eliminate the same frequencies in the PV condition through phase-cancellation. As previously discussed (see, 3.1.2 Apparatus and stimuli), other stimulus properties were either not expected to induce periodic fluctuations or were expected to induce the same periodic fluctuations in both conditions. Therefore, any frequency components with amplitudes significantly higher in the PL than the PV condition should belong to fluctuations induced by the polar angle modulation alone.

We applied a Fourier transform on the time-averaged data (frequency resolution: $1/11 = .09$ Hz), and calculated the baseline-subtracted amplitudes by subtracting from the amplitude of each frequency bin the average amplitude of 16 neighboring bins (8 from both sides), with the exclusion of two immediately adjacent bins (one on each side). Since the dot's polar angle was modulated at 1 Hz, we expected to observe frequency components at 1 Hz and its harmonics. We also compared the overall amplitude of activity distributed across these fundamental and harmonic frequencies. To this end, we summed the baseline-subtracted amplitudes of all harmonic frequencies which were significantly above the noise level (Retter et al., 2021; Retter & Rossion, 2016). Significant harmonics were determined by first grand-averaging the FFT spectra across participants, channels, and conditions, and then calculating Z-scores for each frequency bin with a similar procedure to the baseline-subtracted amplitude calculation (i.e., 16 neighboring bins were used as the baseline for each frequency bin). Only the frequency components up to the sixth harmonic (including the fundamental frequency) passed the threshold of significance ($Z > 1.64$, $p < .05$, one-tailed, signal > noise), and thus were included when calculating the summed baseline-subtracted amplitudes for each condition.

We identified two separate ROIs for our analyses. The first included only the Oz channel, which largely covers V1 where the position-dependent discrepancies across different retinotopic areas, such as cortical magnification, are most well-known (Dahlem & Tusch, 2012; Daniel & Whitteridge, 1961; Dow et al., 1981; Gattass et al., 1987; Palmer et al., 2012; Van Essen et al., 1984). The second ROI consisted of 8 posterior channels (Oz, O1, O2, POz, PO3, PO4, PO7, PO8) which roughly encompasses the occipital-parietal areas in which previous studies consistently found frequency components induced by position-modulated stimuli (Aissani et al., 2011; Alp et al., 2017; Nozaradan et al., 2012; Palomares et al., 2012; Pitchaimuthu et al., 2021; Varlet et al., 2023). Separately for each ROI, we ran a 2-by-2 repeated-measures ANOVA (rm-ANOVA) on participants' summed baseline-subtracted amplitudes with phase (PV *vs* PL) and rotation direction (CW *vs* CCW) as within-subject factors. For the first ROI, the summed baseline-subtracted amplitudes from the Oz channel were used in the rm-ANOVA. For the second ROI, we averaged the summed baseline-subtracted amplitudes from the eight channels to quantify and compare the overall response in these posterior channels. All reported p-values for both tests were Bonferroni-corrected for multiple comparisons (i.e., one for each ROI; Keil et al., 2022).

Lastly, we calculated the SNR (signal/baseline) for all frequency bins using the same baseline as described above, to better illustrate the pattern of harmonic frequencies contained in the evoked signal. SNR is preferred for this purpose as higher frequencies can have a low amplitude (and therefore a low baseline-subtracted amplitude) but still have a high SNR.

3.2. *Results*

3.2.1. *Behavioral results*

The behavioral task in the catch trials served the sole purpose of encouraging participants to pay attention to the stimulus. Therefore, we only required participants to have accuracy above 50% on the catch trials. Overall, participants' accuracy was high ($M = 88.14\%$, $SD = 8.31$), and no participant had below-chance accuracy in either of the two experimental blocks (Min. = 58.33%).

3.2.2. *Frequency domain results*

Z-scores calculated on the grand-averaged amplitude spectra indicated that harmonics of the polar angle modulation frequency were significant up to the sixth harmonic (see, 3.1.6 Frequency domain analysis), thereby constituting our frequencies-of-interest for the following analyses. Fig. 4 illustrates that these six frequencies are clearly distinguishable from noise in the two PL conditions (CW and CCW) whereas they are at noise levels (SNR ≈ 1) in the PV conditions. A visual inspection of the topographical maps (Fig. 5) displaying the summed baseline-subtracted amplitudes for each condition across EEG channels suggests a clear posterior activity in the PL, but not in the PV, conditions.

A rm-ANOVA on the summed baseline-subtracted amplitudes from the Oz channel (i.e., the first ROI) revealed a significant main effect of phase [$F(1, 12) = 86.74$, $p_{bonf} < 10^{-5}$, $\eta^2_p = .878$]. The main effect of rotation direction [$F(1, 12) = .59$,

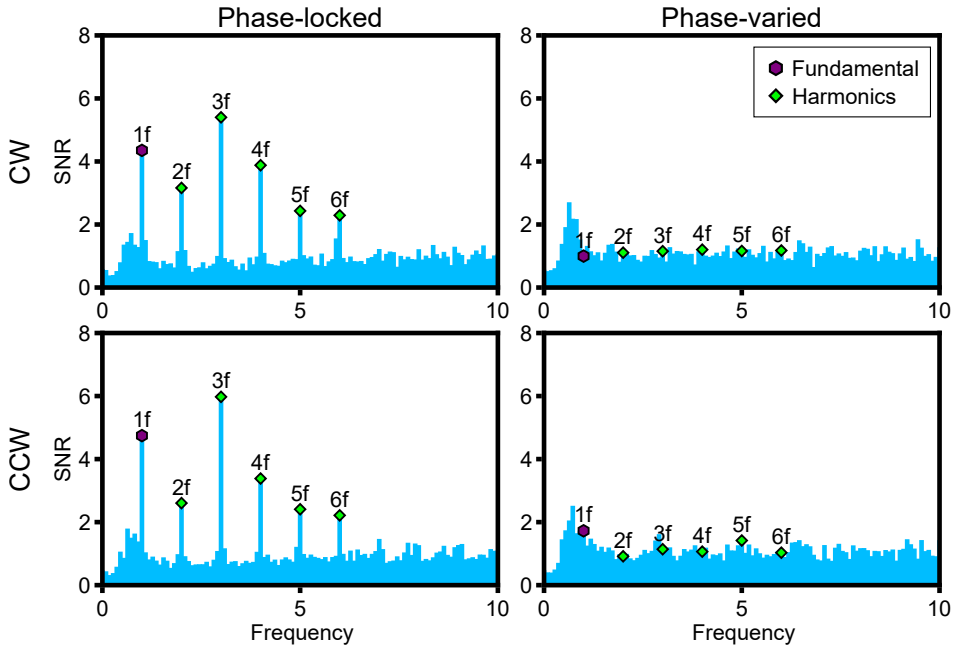

Fig. 4 – FFT signal-to-noise ratio (SNR) spectra. SNR calculated on the FFT amplitude spectra obtained from time-domain averaged trials for each condition. The figures here reflect the SNR values extracted from the Oz channel, averaged across participants. The first six harmonics of the modulation frequency (1*f*, 2*f*, 3*f*, 4*f*, 5*f*, and 6*f*) exhibit high SNR (>2) in the phase-locked conditions, but are at noise levels (~1) in the phase-varied conditions.

p_{bonf} = .91, η^2_p = .047] and the interaction term [$F(1, 12) = 5.86*10^{-5}$, $p_{bonf} = 1$, $\eta^2_p = 4.88*10^{-6}$] were not significant. Fig. 5b depicts the distinction among each condition. Bonferroni-corrected post hoc tests revealed that the summed baseline-subtracted amplitudes from the PL condition were significantly larger than those from the PV condition, within both CW ($M_{diff} = 1.516$, $p_{bonf} < 10^{-5}$) and CCW ($M_{diff} = 1.517$, $p_{bonf} < 10^{-5}$) conditions. CW and CCW conditions did not differ significantly within PV ($M_{diff} = .048$, $p_{bonf} = 1$) or PL ($M_{diff} = .047$, $p_{bonf} = 1$) conditions.

A separate rm-ANOVA on the summed baseline-subtracted amplitudes averaged from the eight posterior channels (i.e., the second ROI) also revealed similar results: The main effect of phase [$F(1, 12) = 75.77$, $p_{bonf} < 10^{-5}$, $\eta^2_p = .863$] was significant, but the main effect of rotation direction [$F(1, 12) = .48$, $p_{bonf} = 1$, $\eta^2_p = .039$] and the interaction term [$F(1, 12) = .064$, $p_{bonf} = 1$, $\eta^2_p = .005$] were not. The PL condition had larger summed baseline-subtracted amplitudes than the PV condition in both CW ($M_{diff} = 1.67$, $p_{bonf} < 10^{-5}$) and CCW ($M_{diff} = 1.69$, $p_{bonf} < 10^{-5}$) conditions (see, Fig. 5b). There was no significant difference between the CW and CCW conditions within PV ($M_{diff} = .05$, $p_{bonf} = 1$) or PL ($M_{diff} = .023$, $p_{bonf} = 1$) conditions.

4. Experiment 2: Eccentricity modulation

Results from Experiment 1 revealed frequency components that are contingent on the phase of the polar angle modulation, and therefore originate from a position-dependent modulation of the EEG signal. These results are in line with our hypothesis that systematic position-dependent discrepancies in the EEG strength can yield frequency components by interacting with a position-modulated stimulus. In Experiment 2, we investigated whether a modulation of stimulus eccentricity can drive similar results.

4.1. *Method*

Materials and methods were identical to Experiment 1, with the exceptions outlined below.

4.1.1. *Participants*

Thirteen Sabancı University students (8 female, 5 male; mean age = 21.38 years, SD = .5) with normal or corrected-to-normal vision were recruited in exchange for course credit. The sample size was based on previous studies as in Experiment 1. A sensitivity analysis revealed that this sample size was sufficiently powered (power = .80) to detect effect sizes larger than .73 (Cohen's d, one-tailed paired-samples *t*-test; see, 4.1.3 Frequency domain analysis).

4.1.2. *Apparatus and stimuli*

In Experiment 2, we employed the same rotating dot stimulus but adjusted the position of the rotation trajectory by shifting it in eight different directions (shift direction angles: 0°–315° in increments of 45°). As a consequence, the center of the rotation trajectory was always positioned 2 dva away from the fixation cross, which allowed the dot's eccentricity to be modulated between 3 and 7 dva during its rotation. The phase of this eccentricity modulation depended on the position from which the dot started its rotation. More

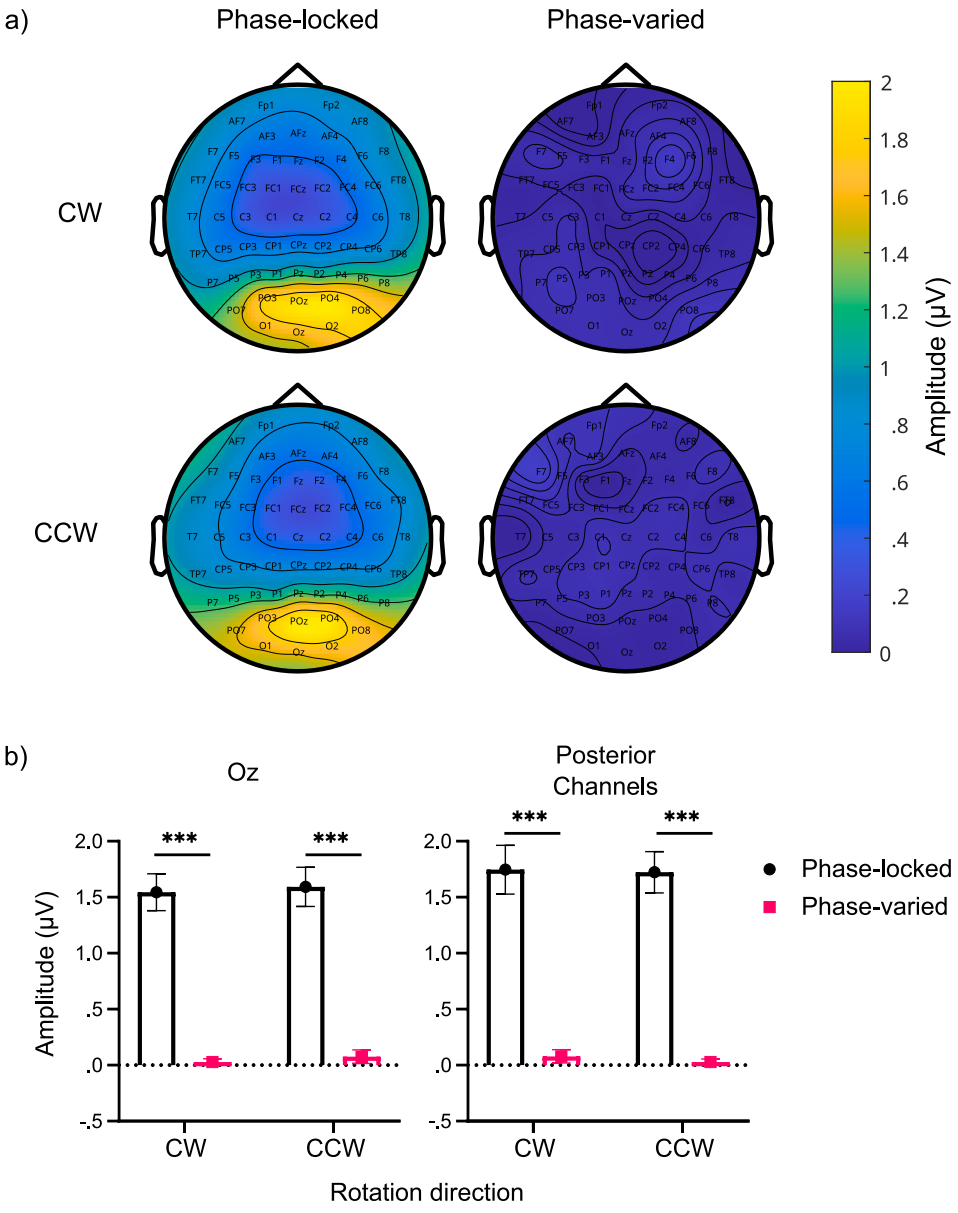

Fig. 5 – Summed baseline-subtracted amplitudes. (a) Topographical plots of grand-averaged summed baseline-subtracted amplitudes of the first six harmonics of the modulation frequency (1*f*, 2*f*, 3*f*, 4*f*, 5*f*, and 6*f*) across all channels. (b) The summed baseline-subtracted amplitudes of the first six harmonics of the modulation frequency are depicted for the two regions-of-interest. Left: Summed baseline-subtracted amplitudes obtained from the Oz channel. Right: Average of the summed baseline-subtracted amplitudes obtained from the eight posterior EEG channels. Error bars indicate the standard error of the mean. Statistical significance is denoted as * ($p < 10^{-5}$).**

specifically, the phase of the eccentricity modulation was determined by the relative angle between the dot's initial position and the axis of the trajectory shift (Fig. 6). Using this property, we kept the phase of the eccentricity modulation constant across trials in the PL eccentricity modulation condition and varied it in the PV condition (range: 0°–315° in steps of 45°). The constant phase used for the eccentricity modulation in the PL condition was randomized between participants by randomly assigning each participant a predetermined relative starting angle. This meant that the relative starting angle of the dot in the PL condition, and therefore the phase of the eccentricity modulation, was different for each participant (but still constant across the PL trials within participants).

Shifting the rotation trajectory in eight different directions allowed for varying the phase of the polar angle modulation in both phase conditions, while still enabling a phase-locked eccentricity modulation in the PL condition.

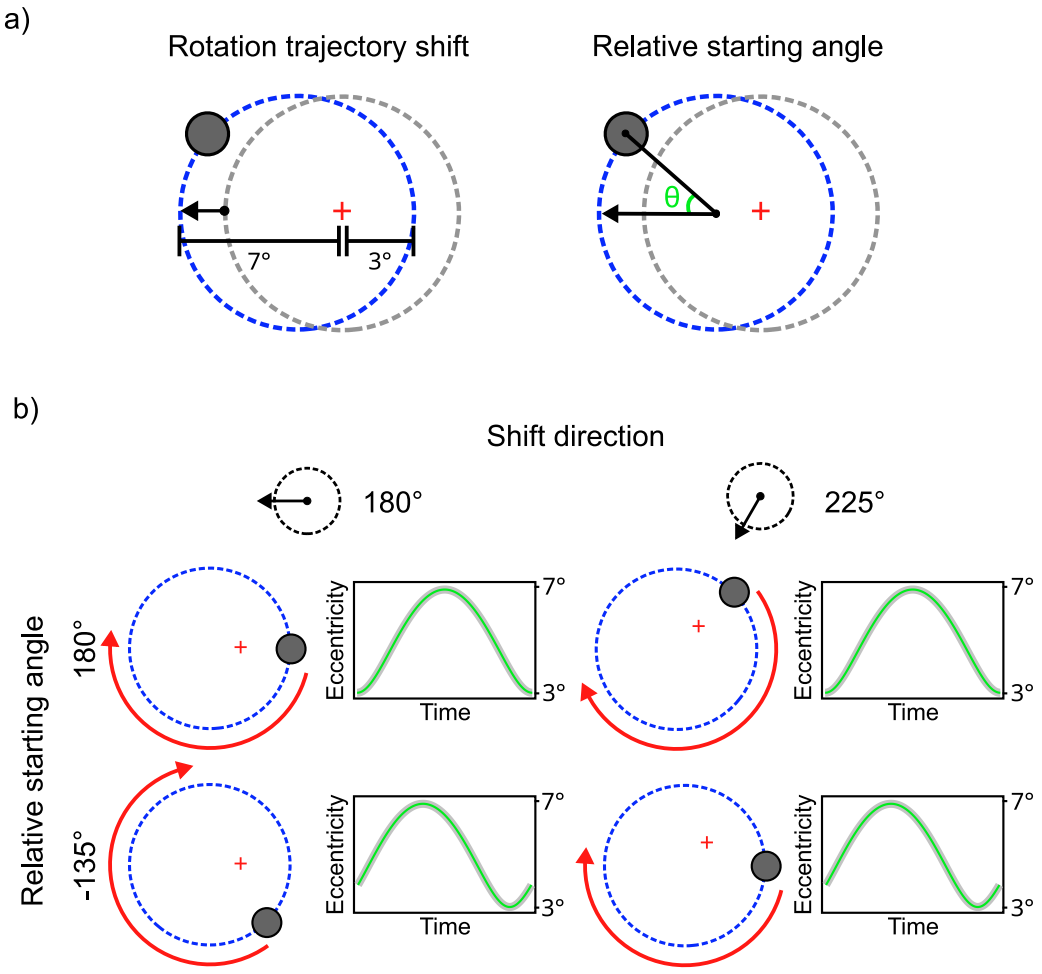

Fig. 6 – Rotation trajectory shift and the phase of the eccentricity modulation. (a) Left: The circular rotation trajectory was shifted by 2 dva. As a result, the dot's eccentricity changed from 3 to 7 dva during its rotation. Right: Relative starting angle of the dot defined as the angle between the vector of the rotation trajectory shift and the dot's initial position (shift angle–dot's polar angle). This relative starting angle determined the phase of the eccentricity modulation. (b) The phase of the eccentricity modulation was determined by the relative starting angle of the dot, even when different shift angles were applied to the rotation trajectories. The left and right columns represent conditions where the rotation trajectories were shifted in different directions, yet the phases of the eccentricity modulation remained the same. This consistency was achieved by maintaining the same relative starting angle across different shift directions.

Therefore, we expected to observe only the frequency components introduced by the eccentricity modulation, as those introduced by the polar angle modulation would be eliminated through phase-cancelation. As a consequence of the cancellation of polar angle-dependent signals, any influence of the dot's rotation direction (CW and CCW) was also expected to be eliminated. Therefore, to increase the number of trials for our phase conditions, we omitted the rotation direction conditions in Experiment 2. Instead, we maintained a constant rotation direction (either CW or CCW) across all trials, with the specific direction randomly predetermined for each participant.

Each trial lasted 10 secs and contained 10 full rotations of the dot. PL and PV conditions were presented in two different blocks similar to Experiment 1. Each block had 76 trials, 12 of which were catch trials. The task in the catch trials was identical to Experiment 1.

4.1.3. *Frequency domain analysis*

Bad channels were interpolated (.5% per subject on average) using neighboring channels, and a small number of trials (M = .96%, SD = 1.15) with hardware-related artifacts were excluded from the analyses. Later, trials from the PL and PV conditions were averaged separately in the time domain (Trial $N \approx 64$). Following the same Z-score calculation procedure and significance criterion as in Experiment 1 (baseline: 14 neighboring bins for each frequency), only the fundamental frequency component (1 Hz) was found significant. Therefore, we used the baseline-subtracted amplitudes of the fundamental frequency to compare the two conditions in two paired-samples t-tests for the two ROIs. Since we expected the

PL condition to produce large baseline-subtracted amplitudes and the PV condition around the noise level (baseline-subtracted amplitude ≈ 0), we ran one-tailed tests.

4.2. Results

4.2.1. Behavioral results

Participants' accuracy on the behavioral task was similar to Experiment 1 ($M = 84.62\%$, $SD = 9.22$, Min. = 58.33%).

4.2.2. Frequency domain results

Z-scores calculated on the grand-averaged amplitude spectra revealed that only the fundamental frequency was significantly larger than the noise ($Z = 2.75$, $p = .003$, one-tailed, signal > noise). Fig. 7 shows that the fundamental frequency had a large SNR in the PL condition, but was at noise levels in the PV condition (SNR ≈ 1). Topographical maps of the baseline-subtracted amplitudes (Fig. 8b) suggest that phase-locked eccentricity modulation elicited activity in the posterior channels, whereas no particular activity was observed in the PV condition.

We ran two separate one-tailed (i.e., PL > PV) paired-samples *t*-tests on the two ROIs. The fundamental frequency had a significantly larger baseline-subtracted amplitude in the PL condition for both the Oz channel ($t(12) = 5.17$, $p_{bonf} < .001$, $d = 1.43$), and the average of the eight posterior channels ($t(12) = 5.12$, $p_{bonf} < .001$, $d = 1.42$), compared to the PV condition (Fig. 8a).

5. Discussion

We hypothesized that position-dependent factors that influence the strength of signals measured from different retinotopic populations (e.g., cortical magnification, cortical volume and depth, dipole orientation of local currents relative to the electrode array, conductivity of brain tissue and cerebrospinal fluid) can, under certain circumstances, introduce systematic signal fluctuations that give rise to frequency components mimicking SSVEP components typically interpreted as signatures of functional processing of periodically modulated stimulus features. To test this, we simulated the influence of such position-dependent structural factors on EEG signals and asked whether signal fluctuations driven purely by these factors could yield frequency components when no other stimulus property was periodically modulated. Our simulations revealed that, even when individual units responding to the stimulus are driven equally across space and time, position-dependent factors interacting with a position-modulated stimulus can generate distinct frequency components that are strictly phase-coupled to the stimulus's position modulation. The specific frequency components produced in this way depend jointly on the trajectory of the position modulation and on the position-dependent weighting of signals from different retinotopic populations (i.e., the Retinotopic Weight Function).

In two subsequent EEG experiments, we tested whether the frequency components generated by position-dependent factors in our simulations can also arise in practice. We modulated the position of a singleton shape by varying its polar angle (Experiment 1) or its eccentricity (Experiment 2). For each type of position modulation, we had a phase-locked (PL) condition, in which the phase of the modulation was identical across trials, and a phase-varied (PV) condition, in which the phase was randomized across trials. All other stimulus properties were kept constant across conditions, such that they would either produce no frequency components or identical components in both conditions. This design allowed us to use trial-averaged phase-cancellation in the PV condition to selectively remove signal fluctuations that were strictly time-locked to the periodic position modulation. Consequently, any frequency components that differed between the PL and PV conditions can be attributed primarily to position-dependent factors interacting with the position-modulated stimulus. In line with this prediction, we observed clear frequency components at the position modulation frequencies in both experiments when the polar angle and eccentricity modulations were phase-locked across trials, whereas the same components were indistinguishable from noise when the phases were randomized.

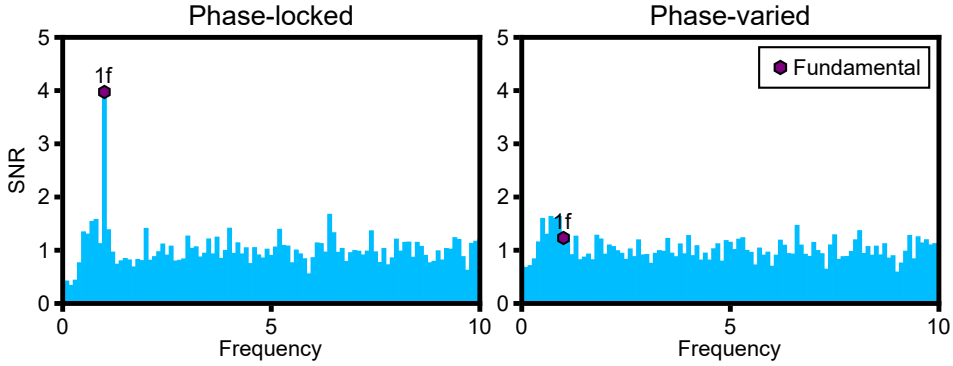

Fig. 7 – FFT signal-to-noise ratio (SNR) spectra. SNR calculated on the FFT amplitude spectra obtained from time-domain averaged trials for each condition, from the Oz channel. The fundamental modulation frequency (1*f*) exhibits a high SNR in the phase-locked condition, whereas its SNR is at noise levels in the phase-varied condition.

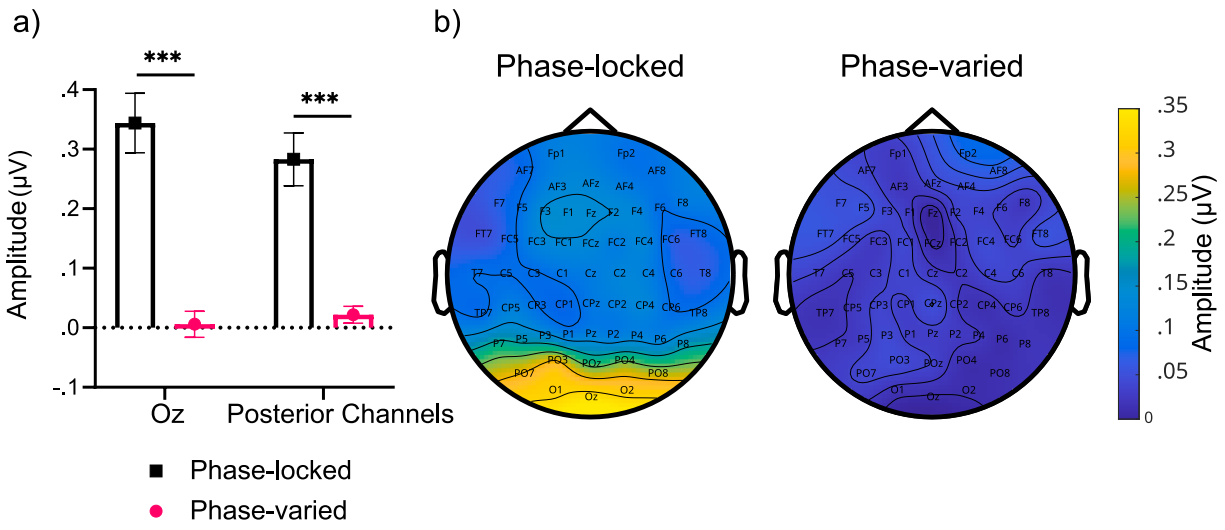

Fig. 8 – Baseline-subtracted amplitudes. (a) The baseline-subtracted amplitudes of the modulation frequency (1*f*) are depicted for the two regions-of-interest: Baseline-subtracted amplitudes obtained from the Oz channel, and average of the baseline-subtracted amplitudes obtained from the eight posterior EEG channels. Error bars indicate the standard error of the mean. Statistical significance is denoted as * ($p < .001$). (b) Topographical maps of grand-averaged baseline-subtracted amplitudes of the fundamental modulation frequency (1*f*) across all channels.**

This position-dependent modulation of the EEG signal can be readily explained by retinotopic differences in cortical and biophysical properties that determine how neural activity is translated into measured signals. For instance, because the visual field is mapped non-uniformly onto the visual cortex and some visual field locations are represented by disproportionately larger or differently arranged cortical areas (i.e., cortical magnification; Daniel & Whitteridge, 1961; Horton & Hoyt, 1991; Schwartz, 1980), the same stimulus can activate more or less brain tissue and thereby produce different signal amplitudes depending on its position in the visual field. Similar position-dependent variation can arise from other structural factors (e.g., cortical depth: Butler et al., 2019; cancellation between simultaneously active sources: Ahlfors et al., 2010; orientation of dipoles relative to electrodes: Capilla et al., 2016), since simple amplification or attenuation of signals across retinotopic areas is sufficient to produce systematic fluctuations as a function of stimulus position. Consequently, any set of structural factors that systematically influences EEG amplitude could generate distinguishable frequency components by introducing position-dependent fluctuations, even when the underlying neuronal responses to the stimulus are equivalent across positions. In such cases, the resulting frequency components would primarily reflect structural weighting rather than modulations in the responses of neurons selectively tuned to a particular stimulus feature.

The key point here is not that any one structural factor solely explains these results, but that such structural factors, either collectively or independently, can generate frequency components that are orthogonal to (and can coexist with) functionally driven sources of periodic EEG signals. This finding refines a common interpretive assumption in many SSVEP applications, which posits that the frequency components observed in response to a periodically modulated stimulus are a direct reflection of evoked neuronal activity processing the specific stimulus property that is modulated (Norcia et al., 2015). In contrast, the frequency components we report can be accounted for without appealing to a specialized neural mechanism tuned to the periodically modulated feature. Instead, they suggest that structural factors can exert a multiplicative influence on signals originating from neural responses to the stimulus, effectively acting as an independent source of amplitude modulation. As a result, while these frequency components may resemble typical SSVEP components, their presence alone does not guarantee that the underlying activity indexes computations on the modulated stimulus property and thus provides limited leverage for inferences about visual processing as they simply emerge as a byproduct of the brain's structural organization.

The brain's structural organization is tightly coupled to its function, and many feature- and category-selective neural populations are anatomically localized. As a result, SSVEP components that differentiate categorical stimuli (for example, faces from objects) can be driven by both functional factors (e.g., the pattern and strength of responses in face- and object-selective populations) and structural factors (e.g., the size and neuronal density of these regions, their cortical depth and orientation, their distance from the electrode array, and other biophysical influences), either independently or in combination. In some paradigms, SSVEPs may even be predominantly shaped by such structural weighting, yet this does not necessarily constitute a problem: these structural influences can provide useful information about the functional localization of specific category-selective mechanisms and can be deliberately exploited for mapping purposes. At the

same time, the same structural dependencies mean that low-level regularities in stimulus design, such as systematic differences in retinotopic position or local variance in spatial frequency, can generate or amplify SSVEP components in a way that mimics higher-level feature- or category-selective responses and thereby becomes a confounding factor. We suggest that researchers should explicitly consider these structural influences when interpreting SSVEP components and decide, on a case-by-case basis, whether they are informative with respect to the functional question at hand or whether they instead obscure the underlying neural mechanisms and thus need to be minimized, counterbalanced, or controlled for.

The frequency components generated by position-dependent factors present a particular challenge when they closely resemble those expected to result from specific neural mechanisms or neural populations that are selective or sensitive to particular stimulus attributes. For instance, in SSVEP studies focusing on visual motion processing, researchers often employ stimuli composed of moving visual elements whose positions undergo repetitive modulation along a fixed path of motion (e.g., Aissani et al., 2011; Nozaradan et al., 2012; Pitchaimuthu et al., 2021; Varlet et al., 2023). Some of these studies have argued that the frequency components elicited in response to such stimuli reflect the modulation in the activity of motion-sensitive neural populations, including those sensitive to motion direction (e.g., Aissani et al., 2011; although their results based on intermodulation components cannot be readily explained by structural factors) or repetitive motion patterns (e.g., Nozaradan et al., 2012; Pitchaimuthu et al., 2021). However, with such motion stimuli, the motion-related characteristics are inherently linked to position modulation. Consequently, position-dependent periodic fluctuations could lead to similar frequency components either independently or in conjunction with the signal fluctuations introduced by the modulated activity of motion-sensitive populations. This complicates the interpretation of results from these studies, making it challenging to attribute the observed frequency components solely to specific neural mechanisms or populations.

Interestingly, our results do not implicate specific neural responses sensitive to repeating motion patterns, or "visual beats", that previous studies have reported (Nozaradan et al., 2012; Pitchaimuthu et al., 2021). In our experiments, the singleton dot stimulus always completed a full cycle every 1 sec in both PL and PV conditions. If there were neural responses specific to the periodicity of motion, we would have observed them in both of our phase conditions. Instead, we only observed significant frequency components when the modulations of stimulus position were phase-locked across trials. This suggests that these frequency components were not driven by neural mechanisms sensitive to the periodicities in motion, but rather by position-dependent modulation of the EEG signal.

Another interesting aspect of our data is the different patterns of frequency components observed for polar angle and eccentricity modulations. The polar angle modulation in Experiment 1 produced complex periodic waveforms containing the first six harmonics of the modulation frequency (1*f*–6*f*), whereas the eccentricity modulation in Experiment 2 yielded a simpler, essentially sinusoidal waveform containing only the fundamental frequency (1*f*). In our simulations, the emerging frequency components always depended on the interaction between the trajectory of the position modulation and the RWF. Assuming that the underlying RWF of the visual system is the same across experiments, the differences in the observed spectra therefore reflect how this common weighting function is sampled by the different position-modulation trajectories.

In Experiment 1, the steady rotation of the stimulus effectively sampled variation in the RWF across polar angle. In Experiment 2, only the sinusoidal eccentricity modulation was PL, which sampled variation in the RWF across the 3–7 dva eccentricity range. Taken together, our results suggest a RWF that is roughly linear across eccentricity and non-linear across polar angle within the spatial range of our position modulations (5 dva for polar angle, 3–7 dva for eccentricity). This pattern is consistent with previous findings that cortical magnification and population receptive field sizes decrease approximately linearly with eccentricity in the central visual field, but vary non-linearly with polar angle (Daniel & Whitteridge, 1961; Dumoulin & Wandell, 2008; Silva et al., 2018), although other structural factors beyond cortical magnification may have also contributed to the differences between the two experiments. Future work could characterize the retinotopic weighting of EEG signals across a broader extent of the visual field and more directly dissociate potential structural influences.

A potential alternative to our account is that the frequency components we observed could have been produced not only by structural factors but also by functional, position-sensitive mechanisms. For example, this would be possible if distinct neural populations are preferentially engaged by the singleton dot at specific absolute locations in the visual field, or if position-sensitive units with relatively large receptive fields systematically modulate their responses according to the dot's instantaneous position. There is at least some evidence consistent with this possibility. For example, the visual system is sensitive to the typical visual field locations of objects, and category-selective responses are enhanced when stimuli appear at their common locations in the visual field (Kaiser et al., 2018). Likewise, object-selective neurons in monkey inferotemporal cortex (analogous to human LOC) exhibit stronger responses to foveal compared to peripheral stimuli (Rolls et al., 2003), indicating a form of functional eccentricity dependence. By analogy, there could be higher-level or intermediate-level visual neurons that respond more strongly to our singleton dot at particular positions or within specific segments of its trajectory, acting as a functional source of position-dependent signal fluctuations. Although this interpretation remains speculative in the context of our simple dot stimulus, it highlights that functional position-sensitive mechanisms could, in principle, have contributed to the frequency components we observed, potentially in combination with the structural position-dependent factors that are the primary focus of our account.

It is important to acknowledge two limitations of our study. First, although participants were explicitly instructed to maintain fixation on a central cross throughout all trials, we did not directly monitor gaze position. If participants

systematically tracked the moving dot with smooth pursuit eye movements or frequent saccades, the stimulus would remain relatively stable in retinal coordinates, thereby reducing the position-dependent differences in signal strength that form the basis of our account. Our interpretation therefore assumes that fixation was maintained to a sufficient degree for the stimulus to traverse different retinotopic regions over time. Second, even if overt eye movements were largely suppressed, the moving dot could still have captured covert attention, modulating activity in retinotopic regions corresponding to its instantaneous position. Our conclusions would remain compatible with such covert attentional modulation if it were relatively uniform across locations; however, a position-dependent attentional mechanism could, in principle, reinforce or partially drive the observed effects. Further work is needed to disentangle potential position-selective attentional contributions from the structural influences highlighted here.

One of the key advantages of SSVEPs is the ability to isolate and track the activity of targeted neural populations that are selectively engaged by specific properties of sensory inputs. However, achieving this requires careful consideration of the targeted neural populations that will be influenced by experimental manipulations, as well as the structural and physical factors governing the translation of neural activity into EEG signals. Our study highlights a scenario in which the observed frequency components do not primarily reflect the selective activity of a specific neural population of interest, but instead capture the inherent discrepancies in EEG strength that vary systematically across different retinotopic areas due to position-dependent factors. In paradigms where spatial and temporal regularities, such as local differences in spatial frequency across stimulus categories or phase-aligned retinal positions of moving stimuli, co-vary with the main experimental manipulations, structural influences can contribute to differences in SSVEP power across conditions or even generate identifiable frequency components in the absence of any underlying selective computation, thereby making it more challenging to attribute observed effects to functional neural mechanisms.

Importantly, we do not view our results as incompatible with the extensive literature demonstrating feature- and category-selective SSVEP components (e.g., Boylan et al., 2023; Kohler et al., 2016; Rossion et al., 2015). Rather, our findings delineate a complementary scenario in which narrowband frequency components can be generated mainly by position-dependent structural factors, provided that spatial regularities are periodic and phase-aligned across trials. In such cases, structural influences can mimic the spectral signatures typically attributed to selectively tuned neural populations and thereby introduce interpretive ambiguity. We therefore do not argue against the view that SSVEPs often index functional neural processing of modulated stimulus features; instead, we highlight that this interpretation is not guaranteed in the presence of systematic spatial regularities. From this perspective, our results motivate spatially informed methodological controls such as minimizing or counterbalancing phase-aligned spatiotemporal regularities as a necessary complement to functional interpretations of SSVEPs. In our PV conditions, we randomized the phase of our position modulations while keeping the other stimulus properties synchronized across trials. This enabled us to eliminate the frequency components arising from position modulation through phase-cancellation. Future studies can apply similar phase-cancellation approaches, along with spatial controls such as collapsing signals across stimulus variations in retinal size, position, and rotation, to more effectively isolate the primary activity of interest from position-dependent influences.

CRediT authorship contribution statement

Ilker Duymaz: Conceptualization, Data curation, Formal analysis, Investigation, Methodology, Software, Visualization, Writing – original draft, Writing – review & editing. **Naoki Kogo**: Conceptualization, Formal analysis, Methodology, Writing – review & editing. **Nihan Alp**: Conceptualization, Formal analysis, Funding acquisition, Methodology, Project administration, Supervision, Writing – review & editing

Acknowledgments

This study was supported by the TUBİTAK 3501 Career Development Grant (220K038) awarded to NA by the Scientific and Technological Research Institution of Turkey.

Scientific transparency statement

DATA: All raw and processed data supporting this research are publicly available: https://doi.org/10.5281/zenodo.18242781.

CODE: All analysis code supporting this research is publicly available: https://doi.org/10.5281/zenodo.18242781.

MATERIALS: All study materials supporting this research are publicly available: https://doi.org/10.5281/zenodo.18242781.

DESIGN: This article reports, for all studies, how the author(s) determined all sample sizes, all data exclusions, all data inclusion and exclusion criteria, and whether inclusion and exclusion criteria were established prior to data analysis.

PRE-REGISTRATION: No part of the study procedures was pre-registered in a time-stamped, institutional registry prior to the research being conducted. No part of the analysis plans was pre-registered in a time-stamped, institutional registry prior to the research being conducted.

For full details, see the *Scientific Transparency Report* in the supplementary data to the online version of this article.

Supplementary data

Supplementary data to this article can be found online at https://doi.org/10.1016/j.cortex.2026.03.005.

REFERENCES

Ahlfors, S. P., Han, J., Lin, F.-H., Witzel, T., Belliveau, J. W., Hämäläinen, M. S., & Halgren, E. (2010). Cancellation of EEG and MEG signals generated by extended and distributed sources. *Human Brain Mapping, 31*(1), 140–149. https://doi.org/10.1002/hbm.20851

Aissani, C., Cottereau, B., Dumas, G., Paradis, A.-L., & Lorenceau, J. (2011). Magnetoencephalographic signatures of visual form and motion binding. *Brain Research, 1408*, 27–40. https://doi.org/10.1016/j.brainres.2011.05.051

Allen, D., Tyler, C. W., & Norcia, A. M. (1996). Development of grating acuity and contrast sensitivity in the central and peripheral visual field of the human infant. *Vision Research, 36*(13), 1945–1953. https://doi.org/10.1016/0042-6989(95)00257-x

Allman, J. M., & Kaas, J. H. (1971). Representation of the visual field in striate and adjoining cortex of the owl monkey (Aotus trivirgatus). *Brain Research, 35*(1), 89–106. https://doi.org/10.1016/0006-8993(71)90596-8

Alp, N., Kogo, N., Van Belle, G., Wagemans, J., & Rossion, B. (2016). Frequency tagging yields an objective neural signature of Gestalt formation. *Brain and Cognition, 104*, 15–24. https://doi.org/10.1016/j.bandc.2016.01.008

Alp, N., Kohler, P. J., Kogo, N., Wagemans, J., & Norcia, A. M. (2018). Measuring integration processes in visual symmetry with frequency-tagged EEG. *Scientific Reports, 8*(1). https://doi.org/10.1038/s41598-018-24513-w. Article 1.

Alp, N., Nikolaev, A. R., Wagemans, J., & Kogo, N. (2017). EEG frequency tagging dissociates between neural processing of motion synchrony and human quality of multiple point-light dancers. *Scientific Reports, 7*(1), Article 44012. https://doi.org/10.1038/srep44012

Alp, N., & Ozkan, H. (2022). Neural correlates of integration processes during dynamic face perception. *Scientific Reports, 12*(1). https://doi.org/10.1038/s41598-021-02808-9. Article 1.

Boylan, M. R., Panitz, C., Tebbe, A.-L., Vieweg, P., Forschack, N., Müller, M. M., & Keil, A. (2023). Feature-based attentional amplitude modulations of the steady-state visual evoked potentials reflect blood oxygen level dependent changes in feature-sensitive visual areas. *Journal of Cognitive Neuroscience, 35*(9), 1493–1507. https://doi.org/10.1162/jocn_a_02030

Butler, R., Bernier, P.-M., Mierzwinski, G. W., Descoteaux, M., Gilbert, G., & Whittingstall, K. (2019). Cortical distance, not cancellation, dominates inter-subject EEG gamma rhythm amplitude. *Neuroimage, 192*, 156–165. https://doi.org/10.1016/j.neuroimage.2019.03.010

Capilla, A., Melcón, M., Kessel, D., Calderón, R., Pazo-Álvarez, P., & Carretié, L. (2016). Retinotopic mapping of visual event-related potentials. *Biological Psychology, 118*, 114–125. https://doi.org/10.1016/j.biopsycho.2016.05.009

Dahlem, A. M., & Tusch, J. (2012). Predicted selective increase of cortical magnification due to cortical folding. *The Journal of Mathematical Neuroscience, 2*(1), Article 14. https://doi.org/10.1186/2190-8567-2-14

Daniel, P. M., & Whitteridge, D. (1961). The representation of the visual field on the cerebral cortex in monkeys. *The Journal of Physiology, 159*(2), 203–221.

Delorme, A., & Makeig, S. (2004). EEGLAB: An open source toolbox for analysis of single-trial EEG dynamics including independent component analysis. *Journal of Neuroscience Methods, 134*(1), 9–21. https://doi.org/10.1016/j.jneumeth.2003.10.009

Dow, B. M., Snyder, A. Z., Vautin, R. G., & Bauer, R. (1981). Magnification factor and receptive field size in foveal striate cortex of the monkey. *Experimental Brain Research, 44*(2), 213–228. https://doi.org/10.1007/BF00237343

Dumoulin, S. O., & Wandell, B. A. (2008). Population receptive field estimates in human visual cortex. *Neuroimage, 39*(2), 647–660. https://doi.org/10.1016/j.neuroimage.2007.09.034

Faul, F., Erdfelder, E., Lang, A.-G., & Buchner, A. (2007). G*Power 3: A flexible statistical power analysis program for the social, behavioral, and biomedical sciences. *Behavior Research Methods, 39*(2), 175–191. https://doi.org/10.3758/BF03193146

Gattass, R., Sousa, A. P. B., & Rosa, M. G. P. (1987). Visual topography of V1 in the Cebus monkey. *Journal of Comparative Neurology, 259*(4), 529–548. https://doi.org/10.1002/cne.902590404

Gundlach, C., & Müller, M. M. (2013). Perception of illusory contours forms intermodulation responses of steady state visual evoked potentials as a neural signature of spatial integration. *Biological Psychology, 94*(1), 55–60. https://doi.org/10.1016/j.biopsycho.2013.04.014

Horton, J. C., & Hoyt, W. F. (1991). The representation of the visual field in human striate cortex. A revision of the classic Holmes map. *Archives of Ophthalmology (Chicago, Ill.: 1960), 109*(6), 816–824. https://doi.org/10.1001/archopht.1991.01080060080030

Kaiser, D., Moeskops, M. M., & Cichy, R. M. (2018). Typical retinotopic locations impact the time course of object coding. *Neuroimage, 176*, 372–379. https://doi.org/10.1016/j.neuroimage.2018.05.006

Keil, A., Bernat, E. M., Cohen, M. X., Ding, M., Fabiani, M., Gratton, G., Kappenman, E. S., Maris, E., Mathewson, K. E., Ward, R. T., & Weisz, N. (2022). Recommendations and publication guidelines for studies using frequency domain and time-frequency domain analyses of neural time series. *Psychophysiology, 59*(5), Article e14052. https://doi.org/10.1111/psyp.14052

Kohler, P. J., Clarke, A., Yakovleva, A., Liu, Y., & Norcia, A. M. (2016). Representation of maximally regular textures in human visual cortex. *The Journal of Neuroscience, 36*(3), 714–729. https://doi.org/10.1523/JNEUROSCI.2962-15.2016

Liu, S., Zhang, D., Liu, Z., Liu, M., Ming, Z., Liu, T., Suo, D., Funahashi, S., & Yan, T. (2022). Review of brain–computer interface based on steady-state visual evoked potential. *Brain Science Advances, 8*(4), 258–275. https://doi.org/10.26599/BSA.2022.9050022

Norcia, A. M., Gregory Appelbaum, L., Ales, J. M., Cottereau, B. R., & Rossion, B. (2015). The steady-state visual evoked potential in vision research: A review. *Journal of Vision, 15*(6), 1–46. https://doi.org/10.1167/15.6.4

Nozaradan, S., Peretz, I., & Mouraux, A. (2012). Steady-state evoked potentials as an index of multisensory temporal binding. *Neuroimage, 60*(1), 21–28. https://doi.org/10.1016/j.neuroimage.2011.11.065

Oostenveld, R., Fries, P., Maris, E., & Schoffelen, J.-M. (2010). FieldTrip: Open source software for advanced analysis of MEG, EEG, and invasive electrophysiological data. *Computational Intelligence and Neuroscience, 2011*, Article e156869. https://doi.org/10.1155/2011/156869

Palmer, C. R., Chen, Y., & Seidemann, E. (2012). Uniform spatial spread of population activity in primate parafoveal V1. *Journal of Neurophysiology, 107*(7), 1857–1867. https://doi.org/10.1152/jn.00117.2011

Palomares, M., Ales, J. M., Wade, A. R., Cottereau, B. R., & Norcia, A. M. (2012). Distinct effects of attention on the neural responses to form and motion processing: A SSVEP source-imaging study. *Journal of Vision, 12*(10), Article 15. https://doi.org/10.1167/12.10.15

Peirce, J., Gray, J. R., Simpson, S., MacAskill, M., Höchenberger, R., Sogo, H., Kastman, E., & Lindeløv, J. K. (2019). PsychoPy2: Experiments in behavior made easy. *Behavior Research*

Methods, 51(1), 195–203. https://doi.org/10.3758/s13428-018-01193-y

Pitchaimuthu, K., Dormal, G., Sourav, S., Shareef, I., Rajendran, S. S., Ossandón, J. P., Kekunnaya, R., & Röder, B. (2021). Steady state evoked potentials indicate changes in nonlinear neural mechanisms of vision in sight recovery individuals. *Cortex; A Journal Devoted to the Study of the Nervous System and Behavior*, *144*, 15–28. https://doi.org/10.1016/j.cortex.2021.08.001

Quek, G. L., & Peelen, M. V. (2020). Contextual and spatial associations between objects interactively modulate visual processing. *Cerebral Cortex*, *30*(12), 6391–6404. https://doi.org/10.1093/cercor/bhaa197

Regan, D. (1977). Steady-state evoked potentials. *Journal of the Optical Society of America*, *67*(11), 1475–1489. https://doi.org/10.1364/josa.67.001475

Retter, T. L., & Rossion, B. (2016). Uncovering the neural magnitude and spatio-temporal dynamics of natural image categorization in a fast visual stream. *Neuropsychologia*, *91*, 9–28. https://doi.org/10.1016/j.neuropsychologia.2016.07.028

Retter, T. L., Rossion, B., & Schiltz, C. (2021). Harmonic Amplitude Summation for Frequency-tagging Analysis. *Journal of Cognitive Neuroscience*, *33*(11), 2372–2393. https://doi.org/10.1162/jocn_a_01763.

Rice, J. K., Rorden, C., Little, J. S., & Parra, L. C. (2013). Subject position affects EEG magnitudes. *Neuroimage*, *64*, 476–484. https://doi.org/10.1016/j.neuroimage.2012.09.041

Rolls, E. T., Aggelopoulos, N. C., & Zheng, F. (2003). The receptive fields of inferior temporal cortex neurons in natural scenes. *The Journal of Neuroscience*, *23*(1), 339–348. https://doi.org/10.1523/JNEUROSCI.23-01-00339.2003

Rossion, B., Torfs, K., Jacques, C., & Liu-Shuang, J. (2015). Fast periodic presentation of natural images reveals a robust face-selective electrophysiological response in the human brain. *Journal of Vision*, *15*(1), Article 18. https://doi.org/10.1167/15.1.18

Sartucci, F., Borghetti, D., Bocci, T., Murri, L., Orsini, P., Porciatti, V., Origlia, N., & Domenici, L. (2010). Dysfunction of the magnocellular stream in Alzheimer's disease evaluated by pattern electroretinograms and visual evoked potentials. *Brain Research Bulletin*, *82*(3), 169–176. https://doi.org/10.1016/j.brainresbull.2010.04.001

Schaul, N. (1998). The fundamental neural mechanisms of electroencephalography. *Electroencephalography and Clinical Neurophysiology*, *106*(2), 101–107. https://doi.org/10.1016/S0013-4694(97)00111-9

Schwartz, E. L. (1980). Computational anatomy and functional architecture of striate cortex: A spatial mapping approach to perceptual coding. *Vision Research*, *20*(8), 645–669. https://doi.org/10.1016/0042-6989(80)90090-5

Silberstein, R. B., Line, P., Pipingas, A., Copolov, D., & Harris, P. (2000). Steady-state visually evoked potential topography during the continuous performance task in normal controls and schizophrenia. *Clinical Neurophysiology*, *111*(5), 850–857. https://doi.org/10.1016/S1388-2457(99)00324-7

Silva, M. F., Brascamp, J. W., Ferreira, S., Castelo-Branco, M., Dumoulin, S. O., & Harvey, B. M. (2018). Radial asymmetries in population receptive field size and cortical magnification factor in early visual cortex. *Neuroimage*, *167*, 41–52. https://doi.org/10.1016/j.neuroimage.2017.11.021

Slotnick, S. D., Klein, S. A., Carney, T., & Sutter, E. E. (2001). Electrophysiological estimate of human cortical magnification. *Clinical Neurophysiology*, *112*(7), 1349–1356. https://doi.org/10.1016/S1388-2457(01)00561-2

Talbot, S. A., & Marshall, W. H. (1941). Physiological studies on neural mechanisms of visual localization and discrimination. *American Journal of Ophthalmology*, *24*(11), 1255–1264. https://doi.org/10.1016/S0002-9394(41)91363-6

Trimble, C. R. (1968). What is signal averaging. *Hewlett-Packard Journal*, *19*(8), 2–7.

Van Essen, D. C., Newsome, W. T., & Maunsell, J. H. (1984). The visual field representation in striate cortex of the macaque monkey: Asymmetries, anisotropies, and individual variability. *Vision Research*, *24*(5), 429–448. https://doi.org/10.1016/0042-6989(84)90041-5

Varlet, M., Nozaradan, S., Schmidt, R. C., & Keller, P. E. (2023). Neural tracking of visual periodic motion. *European Journal of Neuroscience*, *57*(7), 1081–1097. https://doi.org/10.1111/ejn.15934

Wandell, B. A., Dumoulin, S. O., & Brewer, A. A. (2007). Visual field maps in human cortex. *Neuron*, *56*(2), 366–383. https://doi.org/10.1016/j.neuron.2007.10.012